Published in final edited form as:
ACS Nano. 2010 July 27; 4(7): 3845–3852. doi:10.1021/nn100511a.

A One-Step, Solvothermal Reduction Method for Producing Reduced Graphene Oxide Dispersions in Organic Solvents

Sergey Dubin[†], **Scott Gilje**[‡,*], **Kan Wang**[†], **Vincent C. Tung**[†], **Kitty Cha**[†], **Anthony S. Hall**[†], **Jabari Farrar**[‡], **Rupal Varshneya**[‡], **Yang Yang**[†], and **Richard B. Kaner**[†]

[†]Department of Chemistry and Biochemistry and California NanoSystems Institute, University of California, Los Angeles, California 90095

[‡]Northrop Grumman Aerospace Research Laboratories, Northrop Grumman Corporation, Redondo Beach, California 90278

Abstract

Refluxing graphene oxide (GO) in *N*-methyl-2-pyrrolidinone (NMP) results in deoxygenation and reduction to yield a stable colloidal dispersion. The solvothermal reduction is accompanied by a color change from light brown to black. Atomic force microscopy (AFM) and scanning electron microscopy (SEM) images of the product confirm the presence of single sheets of the solvothermally reduced graphene oxide (SRGO). X-ray photoelectron spectroscopy (XPS) of SRGO indicates a significant increase in intensity of the C=C bond character, while the oxygen content decreases markedly after the reduction is complete. X-ray diffraction analysis of SRGO shows a single broad peak at 26.24° 2θ (3.4 Å), confirming the presence of graphitic stacking of reduced sheets. SRGO sheets are redispersible in a variety of organic solvents, which may hold promise as an acceptor material for bulk heterojunction photovoltaic cells, or electromagnetic interference shielding applications.

Keywords

graphene; graphite oxide; solvothermal; reduced graphene oxide; composite; solar cell; reduction

Graphene oxide (GO) is an atomically thin, water-dispersible platelet material, resulting from the treatment of graphite with powerful oxidizing agents.[1,2] During oxidation, the graphene sheets—of which the bulk graphite is composed—become functionalized with hydroxyl and epoxide groups on their basal plane, while the edges are decorated with carbonyl and carboxyl groups.[3–5] Several authors have reported the ability to reduce GO to graphene-like carbon sheets through the application of either thermal treatment[6–8] or chemical reducing agents,[9–17] which in turn led to speculation that GO could find use as a precursor in a bulk route to graphene sheets.[10,14,18] Several groups have succeeded in creating conducting polymer composites, transparent conducting films, and simple electronic devices based on reduced GO.[17,19–31] In addition to the chemical reduction, Aksay *et al.* have reported the thermal deoxygenation of GO, by rapidly heating samples up to 1100 °C in an inert atmosphere as a route to partially “functionalized” graphene sheets.[7,32] These organic solvent-dispersible sheets have enabled the direct creation of polymer composites without the need for surfactants.[33] Recently, Chen *et al.* have investigated the possibility of using isocyanate-modified graphite oxide as an acceptor

*Address correspondence to s.gilje@ngc.com.

material in bulk heterojunction organic photovoltaic cell devices.[34] The device efficiency reported was 1.1% for samples annealed at 160 °C, which is an order of magnitude improvement from non-annealed devices. The authors explain this phenomenon as a loss of oxygen-containing functional groups from isocyanate-treated graphite oxide and subsequent recovery of aromatic regions. Unfortunately, the annealing temperature cannot exceed 160 °C, due to device constraints, and most of the oxygen-containing functionalities are not removed before 200 °C, potentially limiting the device efficiency.[35]

Although several authors have reported organic dispersions of graphene-like materials, most of these methods utilize strong reducing agents such as hydrazine to achieve high conductivity.[36,37] The use of hydrazine could be problematic for the use of GO-derived graphitic materials for a number of reasons: (1) Being a powerful reducing agent, hydrazine is corrosive and highly flammable, thus posing a potential health hazard to personnel and an environmental hazard for facilities that might produce hydrazine-reduced GO.[38] These hazards could significantly increase the cost of producing reduced graphite oxide (RGO)-based materials on an industrial scale. (2) Trace amounts of hydrazine could be detrimental to some applications such as organic solar cells, where reducing agents such as hydrazine could reduce solar cell donor compounds like poly(3-hexylthiophene), thus increasing the complexity of photovoltaic cell manufacturing.[38] (3) Eliminating hydrazine from the production process would ease the integration of graphene dispersions into current manufacturing processes such as spray-on coatings. Here we report a simple one-step solvothermal approach to synthesizing organically dispersible graphitic platelets from GO that is hydrazine-free.

Our solvothermal reduction method utilizes the high boiling point of *N*-methyl-2-pyrrolidinone (NMP) in combination with the oxygen-scavenging properties of NMP at high temperatures to deoxygenate GO.[39,40] This combination of thermal and chemical deoxygenation yields C/O ratios for the resulting solvothermally reduced graphene oxide (SRGO) that are very similar to those for the hydrazine-reduced GO. In addition to simply deoxygenating GO to produce a more conducting graphitic material, NMP also serves as a dispersing agent for the resulting SRGO sheets by forming strong NMP–GO sheet interactions, thus allowing the sheets to be dispersed in any NMP miscible solvents. Applications that can take advantage of the suggested synthesis include bulk heterojunction (BHJ) solar cells, where SRGO sheets can be mixed with P3HT and act as an acceptor component of the BHJ photovoltaic cell. Papers obtained through filtration or casting of layered SRGO platelets could potentially be used in place of copper as electromagnetic interference (EMI) shielding materials for signal carrying cables. This is of particular importance in aerospace applications where the lower density of carbon-based materials could lead to significant weight savings over current copper braids. By switching to a carbon-based shielding material, a weight saving of several hundred pounds could be achieved for satellite payloads and several thousand pounds for commercial aircraft.[41] Given the current cost of launching payloads into orbit (~$10 000 USD/lb), this could greatly impact the cost of future space launches.

RESULTS AND DISCUSSION

Filtering the SRGO dispersion yields a paper-like material that can be dispersed into organic solvents (Figure 1). Stable colloidal dispersions can be achieved with dimethylsulfoxide (DMSO), ethyl acetate, acetonitrile, ethanol, tetrahydrofuran (THF), dimethylformamide (DMF), chloroform, and acetone with minimal precipitation at 1 mg/mL after 6 weeks. SRGO does not disperse in toluene or dichlorobenzene, but instead, flocculation was observed shortly after sonicating for 3 h. The forces keeping the sheets dispersed in organic solvents likely arise from the miscibility between NMP molecules, which form hydrogen

bonds to residual oxygen functionalities on SRGO sheets, and organic solvents. A previous report[42] indicates that NMP forms hydrogen bonds with the conducting polymer polyaniline; hence we suggest that a similar interaction takes place here. To test this hypothesis, we added a few drops of hydrochloric acid solution to several organic solutions, among them NMP, DMF, and DMSO. This resulted in agglomeration and precipitation of SRGO sheets. These experiments strongly suggest that hydrogen bonding between SRGO sheets and NMP is responsible for the stability of the colloidal suspensions.

While hydrogen bonds can account for the stability of SRGO sheets in NMP, DMF, and DMSO, it still does not offer a reason why synthesis carried out in DMF, DMSO, glycerol, and hexamethylphosphoramide (HMPA) results in agglomerated sheets instead of colloidal dispersions. However, note that all of these chemicals are high boiling point solvents and refluxing at high temperatures is necessary to remove any water molecules bound through hydrogen bonds to graphene oxide. In addition, all of the solvents provide means for hydrogen bonding to various degrees, in order to prevent an agglomeration of the sheets in the absence of water. We suspect the answer may be the fact that NMP, unlike other solvents listed above, has a surface energy that closely matches that of graphene sheets allowing exfoliated sheets to stay in dispersion.[43] NMP has also been suggested to causes cleavage of carbon–oxygen bonds in coals when used under refluxing conditions.[39] In these reactions, a hydroperoxide is thought to be an intermediate in the reaction of NMP and oxygen-yielding *N*-methylsuccinimide.[40] In our experiments, pure NMP changes color from clear to brown when refluxed under atmospheric oxygen. We attribute the color change of NMP in the presence of oxygen to oligomer formation, which has been reported previously.[40] Filtration of SRGO from the reaction mixture yields a dark brown solution, indicating that oxygen is present in the mixture and oligomer formation has occurred. It is unclear at this point what role the oligomer formation plays in the reduction of GO or its ability to form colloidal dispersions of SRGO. Our experiments show that it is imperative to use anhydrous and degassed NMP for the reaction with graphene oxide in order to prevent the self-oligomerization of NMP.

Atomic force microscopy (AFM) was used to analyze SRGO sheets cast onto a silicon substrate from a dispersion of SRGO platelets in DMF. Figure 2a shows an AFM image of SRGO sheets deposited from a 1 mg/mL DMF dispersion onto a Si substrate. Figure 2b shows a 0.93 nm step height from the surface of the substrate to the sheet. The theoretical step height for a single graphene sheet is 0.34 nm; however, this is only observed when sheets are removed from HOPG or other highly crystalline graphite, by means such as peeling with cellophane tape.[44] RGO obtained from hydrazine has been measured to have a step height in the range of 0.6 to 1.0 nm. We believe the sheets measured using AFM in Figure 2a to be single SRGO sheets; however, AFM measurements alone do not provide conclusive evidence that single RGO sheets are obtained using the solvothermal process. We speculate that the increased step height of hydrazine RGO (HRGO) may be attributed to residual functionality on the surface of the sheet, causing some corrugation in the surface of the sheet.[7] Figure 2c presents a scanning electron microscope (SEM) image of a 1 mg/mL acetone SRGO dispersion deposited onto a Si substrate. The image illustrates that the SRGO sheets are distributed across the Si substrate. The inset in Figure 2c shows a higher magnification photograph of a single sheet as deposited onto the Si substrate.

Figure 3a is an SEM image of the cross-sectional area of a piece of air-dried SRGO paper obtained by filtration of an SRGO dispersion in NMP that shows the layer structure of these materials. The inset image in Figure 3a is a photograph of an SRGO paper exhibiting a shiny, black appearance with a metallic luster. SRGO papers were thermally annealed at 1000 °C under an argon atmosphere to drive off any unreacted contaminants. After

annealing, we see that the layered structure is preserved (Figure 3b). This demonstrates that the SRGO platelets are thermally stable in the absence of oxygen.

An X-ray diffraction (XRD) pattern of the GO paper (Figure 4a, middle) exhibits a single peak at 11.26° 2θ corresponding to an interlayer *d* spacing of 7.85 Å. This can be attributed to the expansion of the 3.4 Å spacing between typical graphene sheets to accommodate the water molecules trapped between oxygen-containing functional groups on graphene oxide sheets.[45–48] In contrast to the XRD pattern of GO paper samples, the XRD pattern of SRGO (Figure 4a, bottom) does not have a peak at 11.26° 2θ yet shows a broad peak at 26.24° 2θ (3.39 Å) well within experimental measurement error for a graphitic peak at 3.35 Å (Figure 4a, top). The width of the SRGO peak in the XRD pattern can be attributed to two factors: first, the small sheet size (1 μm and below) and, second, a relatively short domain order or turbostratic arrangement of SRGO stacked sheets, each of which broadens the XRD peak. In Figure 4b, a thermogravimetric analysis (TGA) plot shows a loss of about 15 wt % before 100 °C, which can be attributed to loss of water molecules from within the stacked graphene oxide sheets. A TGA curve of the SRGO paper, in contrast, shows a smaller mass loss (6%) up to 200 °C, signifying that a smaller amount of water or acetone molecules was trapped within the SRGO structure. Furthermore, the TGA of the SRGO paper shows a mass loss of 20% from 200 to 525 °C, followed by a flattening of the curve at higher temperatures. These preliminary findings suggest the mass loss between 200 and 550 °C may be associated with strongly bound NMP and/or NMP-derived functional group molecules.

The four-point probe electrical conductivity of air-dried SRGO paper was measured to be 3.74×10^2 S/m as indicated in Table 1. On the basis of the TGA data, it is apparent that the SRGO paper still retains a significant portion of NMP, which limits the electrical conductivity. To remove any residual NMP (boiling point = ~203 °C) trapped within the paper samples, three SRGO paper samples were annealed at ~250, 500, and 1000 °C for 12 h in a tube furnace under a flow of helium gas. The samples developed a gray hue and even became lustrous silver as the annealing temperature approached 1000 °C, yet still retained their layered structure, as can be seen in Figure 3b. As we have previously suggested, NMP bonds strongly to carbon networks, necessitating the higher temperatures to remove residual NMP. Previous reports indicate that annealing to 500 °C has been shown to remove up to 95% of the residual NMP. However, by annealing the sample to only 250 °C, we sought to eliminate NMP, without subjecting the sample to significant thermal reduction. As shown in Table 1, the result is an order of a magnitude rise in conductivity from 3.74×10^2 to 1.38×10^3 S/m. This phenomenon can be explained by the interaction of NMP molecules with the surface of the sheets, thus preventing good contact between adjacent sheets. Through the elimination of residual NMP, the contacts between sheets are improved and conductivity increases. Further annealing to 500 °C demonstrates that conductivity will continue to increase, but at a slower rate, reaching 5.33×10^3 S/m. Annealing the sample to 1000 °C further increases the conductivity to 5.73×10^4 S/m, which indicates that a considerable amount of graphitization has taken place.

To further investigate the nature of SRGO, we employed X-ray photoelectron spectroscopy (XPS) to analyze the elemental composition of both reduced and unreduced graphene oxide paper. XPS analysis has been used in the past to determine atomic composition and carbon to oxygen (C/O) ratios of GO and RGO. Reduction of GO to RGO is usually indicated by an increase in the C/O ratio and, in the case of hydrazine reduction, uptake of some nitrogen.[18] Figure 5 is a comparison of XPS spectra of GO to the SRGO paper, exhibiting a decreased peak intensity for all oxygen-containing functional groups yet an increase in peak intensity for the C–C bond.[46,49] Additionally, SRGO exhibited a peak at 285.8 eV, corresponding to a carbon–nitrogen bond. It is possible that SRGO sheets have attained a certain amount of carbon–nitrogen bonds through functionalization during the refluxing in NMP. Although the

SRGO used for XPS analysis had been washed extensively using acetone, some residual NMP could be present at the sheet surface, resulting in the presence of a C–N XPS peak. The exact mechanism of this C–N bond formation is still being investigated, but prior reports indicate that this is not a new phenomenon and has been observed previously.

The results of the XPS analysis are listed in Table 2. The samples tested were obtained by filtering dispersions of SRGO directly from NMP after the solvothermal reaction to obtain a paper. The SRGO paper was then redispersed in acetone using sonication and filtered a second time to remove impurities. In addition to the solvothermally reduced GO, we also tested GO that had been reduced using the hydrazine reduction method previously reported by Li *et al.*[10] Looking at Table 2, we see that the GO C/O ratio increases from 2.34 to 5.15 after thermal reduction in NMP. Further annealing of SRGO papers at 1000 °C enhances the C/O ratio to 6.03. Papers made from GO platelets that had been reduced using hydrazine exhibited a C/O ratio of 3.64. When the hydrazine RGO papers were annealed at 1000 °C, the C/O ratio reached up to 6.36. We attribute the higher C/O ratio of the SRGO *versus* the hydrazine RGO to the bound functional groups at the surface of the SRGO platelets. When NMP is heated in the absence of GO, the rings typically break open, forming oligomers. In the presence of GO, however, we believe the opened NMP rings functionalize the GO basal planes, thus increasing the carbon content—and C/O ratio—as measured by XPS. When SRGO and hydrazine RGO are annealed, both reduction methods exhibited similar C/O ratios, with hydrazine RGO having a slightly higher ratio over SRGO. If the basal planes in SRGO are in fact being functionalized by NMP, annealing at 1000 °C could serve to drive off this functionality. The results of the XPS data along with the electrical conductivity data indicate that, although the C/O ratio of SRGO is higher, the increase is most likely due to functional groups decorating the surface of the GO sheets and not an improved deoxygenation.

Near-edge X-ray absorption fine structure (NEXAFS) spectroscopy of GO, SRGO, and hydrazine RGO (HRGO) that had been annealed at 1000 °C was performed. Figure 6 shows an overlay plot of the carbon K-edge NEXAFS spectra for the series of RGOs that were treated using different means. At the very bottom of Figure 6 is the carbon K-edge NEXAFS spectrum for pristine GO. The high peak at 284.5 eV corresponds to the $\pi^* \rightarrow 1s$ transition associated with sp^2 carbon content. For the series of spectra in Figure 6, all of the samples tested were measured at a 20° grazing angle, incident to the incoming X-ray beam. Doing so aligns the highly polarized π orbitals to the polarization of the X-ray beam, increasing the measured intensity. Peaks at 287.4 and 288.2 eV correspond to –C–O and –C=O, respectively. In the case of GO, the –C–O peak is taken to represent the C–OH content. Finally, the broad peak located at ~292.7 eV corresponds to the $\pi^* \rightarrow 1s$ associated with sp^3 content. Annealing carbonaceous materials has been known for some time to increase the graphitic content. By annealing the RGOs that had already been reduced by low-temperature thermal or chemical means, we hoped to track changes in the GO crystallinity. From Figure 6, the sp^2 peak appears to be much higher in intensity for the annealed samples *versus* the non-annealed RGOs. In both cases, the annealed samples show fewer oxygen defects due to C–O, as well. Comparing the hydrazine reduction to the solvothermal reduction, it seems that hydrazine yields more sp^2 carbon with less C–O. The reduction in oxygen defects could be due to the preferential attack of hydrazine to ether linkages and epoxide groups present on the graphene oxide surface.

CONCLUSIONS

We have demonstrated a new method for thermally deoxygenating GO to create reduced graphene oxide dispersions without the use of hydrazine as a reducing agent. We believe that the deoxygenation of GO platelets takes place as the result of both thermal

deoxygenation at 200 °C along with a concomitant reaction of GO with NMP molecules.[50] As a result of the surface functionalization, the solvothermally reduced GO platelets remain in a stable dispersion after the reaction. This provides a simple, low-temperature method for reducing GO platelet. Filtration of the SRGO platelets from the reactant NMP mixture removes excess NMP along with oligomer contaminants that form during the reaction. The resulting SRGO material can be redispersed into in a variety of polar organic solvents for potential applications in solar cells or polymer nanocomposites, where traces of hydrazine may prove detrimental for mass production. Filtration of organic SRGO dispersions yields paper materials with an initial conductivity of 3.74×10^2 S/m. With modest heating to 250 °C to remove entrapped solvent, the conductivity of the SRGO paper increases to 1.38×10^3 S/m while preserving the low-temperature benefits of our solvothermal method. Although this conductivity value is not quite as high as the 8.28×10^3 S/m measured for hydrazine-reduced GO, it may be still suitable for a variety of applications such as EMI shielding of signal cables. In this role, SRGO papers could offer suitable shielding but at lower weight than current copper braids; this is especially important in reducing weight in satellites and aircraft. With additional chemical processing, such as oxidative intercalation, it is expected that the conductivity of these SRGO-based papers could be increased even further.

METHODS

In order to generate a stable colloid, a 0.05 wt % GO dispersion in water was sonicated at 50 °C for 60 min using a VWR Ultrasonic Cleaner (B2500A-DTH, 210W) and diluted 1:1 with anhydrous 1-methyl-2-pyrrolidinone (NMP, ACS reagent grade 328634, Sigma-Aldrich). The light brown dispersion obtained was then degassed for 60 min under vacuum to remove any residual atmospheric oxygen present in the mixture. The solution was then purged with argon and placed in a sand bath preheated to 240 °C. The temperature of 240 °C allowed us to reach the reflux faster through rapid elimination of water. The mixture was then allowed to reflux at ~205 °C, as monitored by a mercury thermometer, for 24 h under flowing argon, after which it was filtered through an Anodisc alumina membrane filter (47 mm diameter, 0.2 μm pore size, Whatman International, Maidstone, UK) and washed with pure NMP. The final product was centrifuged at 4500 rpm using a Beckman-Coulter Allegra X-15R centrifuge, saving the supernatant. The supernatant was filtered once again, rinsed with acetone, and allowed to dry on the filter paper under ambient conditions, which will be referred to as the SRGO air-dried paper. Furthermore, several samples of SRGO paper were enclosed in a tube furnace under a flow of helium gas and annealed at temperatures of 250, 500, and 1000 °C. To make organic dispersions, SRGO paper was sonicated at a 1 mg/mL ratio in the following organic solvents for 3 h at 50 °C: dimethylsulfoxide (DMSO), ethyl acetate, acetonitrile, ethanol, tetrahydrofuran (THF), dimethylformamide (DMF), chloroform, acetone, toluene, and dichlorobenzene.

Atomic force microscopy (AFM) measurements were performed in tapping mode on a Multimode atomic force microscope (Nanoscope IIIa, Veeco Instruments) using a silicon tip. Samples were prepared using a 1 mg/mL solution of SRGO in DMF, which was drop-cast onto a freshly cleaned Si substrate and dried in the vacuum oven. Near-edge X-ray absorption spectroscopy (NEXAFS) was taken at Beamline 8-2 Stanford Synchrotron Radiation Lighsource in Menlo Park, CA. X-ray absorbance was measured using total electron yield (TEY) measurement under ultrahigh vacuum conditions. All spectra were plotted by dividing incident intensity (I_o) over TEY output. The spectra were normalized by subtracting a baseline average just before the carbon K-edge and dividing by the integrated intensity of the carbon K-edge peak.

Scanning electron microscope (SEM) analysis was carried out on both the SRGO papers and single sheets. For the cross-sectional analysis of the paper samples, the samples were

mounted on the SEM sample holder parallel to the electron beam. Imaging of single sheets of SRGO and dispersions of SRGO were performed by depositing 1 mg/mL SRGO acetone onto a freshly cleaned Si substrate and allowing the acetone to evaporate. X-ray diffraction (XRD) characterization was performed using SRGO air-dried paper on zero background silicon substrate in a Crystal Logic diffractometer with Ni-filtered Cu Kα radiation (λ = 1.5418 Å). Thermal gravimetric analysis (TGA) of all samples was carried out under an argon gas and a heating rate of 2 °C/min. Photoelectron spectroscopy (XPS) was performed by inserting samples into the analysis chamber of a Thermo VG ESCALAB 250 spectrometer. Spectra were obtained by irradiating each sample with a 320 μm diameter spot of monochromated aluminum Kα X-rays at 1486.6 eV under ultrahigh vacuum conditions. The analysis consisted of acquiring 3–12 scans and signal averaging. The survey scans were acquired with a pass energy of 80 eV, and high-resolution scans were acquired with a pass energy of 20 eV. Electrical measurements were performed using a four-point probe measurement station (Jandel RM3-AR Test Meter with Multiheight Probe attachment), and the average of three data points per sample was recorded.

Acknowledgments

The authors thank Robert Kojima for help carrying out TEM characterization, Julio M. D'Arcy for help with SEM measurements, Matt Allen and Jonathan Wassei for their help in carrying out measurements and intellectual contributions. Funding for this research has been provided by The Northrop Grumman Corporation, Aerospace Systems Sector, Aerospace Research Laboratories (ARL) internal research and development (IRAD) fund and by the Defense Advanced Research Projects Agency (DARPA) Defense Sciences Office (DSO) Contract Number HR0011-09-C-0152, Project Manager(s) Viktoria Greanya/Brian Holloway. Matching support was provided by the University of California Discovery Program (R.B.K.). Additional funding was provided by the Focused Center Research Program Functional Engineered Nano Architectonics (FCRP/FENA) Center (R.B.K.).

REFERENCES AND NOTES

1. Kovtyukhova NI, Ollivier PJ, Martin BR, Mallouk TE, Chizhik SA, Buzaneva EV, Gorchinskiy AD. Layer-by-Layer Assembly of Ultrathin Composite Films from Micron-Sized Graphite Oxide Sheets and Polycations. Chem Mater. 1999; 11:771–778.
2. Brodie BC. On the Atomic Weight of Graphite. Philos Trans R Soc London. 1859; 149:249–259.
3. Lerf A, He H, Forster M, Klinowski J. Structure of Graphite Oxide Revisited. J Phys Chem B. 1998; 102:4477–4482.
4. Cai W, Piner RD, Stadermann FJ, Park S, Shaibat MA, Ishii Y, Yang D, Velamakanni A, An SJ, Stoller M. Synthesis and Solid-State NMR Structural Characterization of ^{13}C-Labeled Graphite Oxide. Science. 2008; 321:1815–1817. [PubMed: 18818353]
5. He H, Riedl T, Lerf A, Klinowski J. Solid-State NMR Studies of the Structure of Graphite Oxide. J Phys Chem. 1996; 100:19954.
6. McAllister MJ, Li JL, Adamson DH, Schniepp HC, Abdala AA, Liu J, Herrera-Alonso M, Milius DL, Car R, Prud'homme RK. Single Sheet Functionalized Graphene by Oxidation and Thermal Expansion of Graphite. Chem Mater. 2007; 19:4396–4404.
7. Schniepp HC, Li JL, McAllister MJ, Sai H, Herrera-Alonso M, Adamson DH, Prud'homme RK, Car R, Saville DA, Aksay IA. Functionalized Single Graphene Sheets Derived from Splitting Graphite Oxide. J Phys Chem B. 2006; 110:8535–8539. [PubMed: 16640401]
8. Zhu Y, Stoller MD, Cai W, Velamakanni A, Piner RD, Chen D, Ruoff RS. Exfoliation of Graphite Oxide in Propylene Carbonate and Thermal Reduction of the Resulting Graphene Oxide Platelets. ACS Nano. 2010; 4:1227–1233. [PubMed: 20112929]
9. Muszynski R, Seger B, Kamat PV. Decorating Graphene Sheets with Gold Nanoparticles. J Phys Chem C. 2008; 112:5263–5266.
10. Li D, Muller MB, Gilje S, Kaner RB, Wallace GG. Processable Aqueous Dispersions of Graphene Nanosheets. Nat Nanotechnol. 2008; 3:101–105. [PubMed: 18654470]
11. Williams G, Serger B, Kamat PV. TiO_2-Graphene Nanocomposites. UV-Assisted Photocatalytic Reduction of Graphene Oxide. ACS Nano. 2008; 2:1487–1491. [PubMed: 19206319]

12. Xu Y, Bai H, Lu G, Li C, Shi GJ. Flexible Graphene Films *via* the Filtration of Water-Soluble Noncovalent Functionalized Graphene Sheets. J Am Chem Soc. 2008; 130:5856–5857. [PubMed: 18399634]
13. Si Y, Samulski ET. Synthesis of Water Soluble Graphene. Nano Lett. 2008; 8:1679–1682. [PubMed: 18498200]
14. Tung VC, Allen MJ, Yang Y, Kaner RB. High- Throughput Solution Processing of Large-Scale Graphene. Nat Nanotechnol. 2008; 4:25–29. [PubMed: 19119278]
15. Stankovich S, Dikin DA, Piner R, Kohlhaas KM, Kleinhammes A, Jia Y, Wu Y, Nguyen ST, Ruoff RS. Synthesis of Graphene-Based Nanosheets *via* Chemical Reduction of Exfoliated Graphite Oxide. Carbon. 2007; 45:1558–1565.
16. Wang G, Yang J, Park J, Wang B, Liu H, Yao JJ. Facile Synthesis and Characterization of Graphene Nanosheets. J Phys Chem C. 2008; 112:8192–8195.
17. Villar-Rodil S, Paredes JI, Martínez-Alonso A, Tascón MD. Preparation of Graphene Dispersion and Graphene–Polymer Composites in Organic Media. J Mater Chem. 2009; 19:3591–3593.
18. Park S, An J, Piner RD, Jung I, Yang D, Velamakanni A, Nguyen ST, Ruoff RS. Aqueous Suspension and Characterization of Chemically Modified Graphene Sheets. Chem Mater. 2008; 20:6592–6594.
19. Gilje S, Han S, Wang MS, Wang KL, Kaner RB. A Chemical Route to Graphene for Device Applications. Nano Lett. 2007; 7:3394–3398. [PubMed: 17944523]
20. Gomez-Navarro C, Weitz RT, Bittner AM, Scolari M, Mews A, Burghrd M, Kern K. Electronic Transport Properties of Individual Chemically Reduced Graphene Oxide Sheets. Nano Lett. 2007; 7:3499–3503. [PubMed: 17944526]
21. Stankovich S, Dikin DA, Dommett GHB, Kohlhaas KM, Zimney EJ, Stach EA, Piner RD, Nguyen ST, Ruoff RS. Graphene-Based Composite Materials. Nature. 2006; 442:282–286. [PubMed: 16855586]
22. Watcharotone S, Dikin DA, Stankovich S, Piner R, Jung I, Dommett GHB, Evmenenko G, Wu SE, Chen SF, Liu CP. Graphene–Silica Composite Thin Films as Transparent Conductors. Nano Lett. 2007; 7:1888–1892. [PubMed: 17592880]
23. Chen H, Muller MB, Gilmore KJ, Wallace GG, Li D. Mechanically Strong, Electrically Conductive, and Biocompatible Graphene Paper. Adv Mater. 2008; 20:3557–3561.
24. Arsat R, Breedon M, Shafiei M, Spizziri PG, Gilje S, Kaner RB, Kalantarzadeh K, Wlodarski W. Graphene-like Nano-Sheets for Surface Acoustic Wave Gas Sensor Applications. Chem Phys Lett. 2008; 467:344–347.
25. Stoller MD, Park S, Zhu Y, An J, Ruoff RS. Graphene-Based Ultracapacitors. Nano Lett. 2008; 8:3498–3502. [PubMed: 18788793]
26. Cote LJ, Kim F, Huang J. Langmuir-Blodgett Assembly of Graphite Oxide Single Layers. J Am Chem Soc. 2009; 131:1043–1049. [PubMed: 18939796]
27. Eda G, Lin YY, Miller S, Chen CW, Su WF, Chhowalla M. Transparent and Conducting Electrodes for Organic Electronics from Reduced Graphene Oxide. Appl Phys Lett. 2008; 92:233305.
28. Wang X, Zhi L, Tsao N, Tomovic Z, Li J, Muller K. Transparent Carbon Films as Electrodes in Organic Solar Cells. Angew Chem, Int Ed. 2008; 47:2990–2992.
29. Wu J, Becerril HA, Bao Z, Liu Z, Chen Y, Peumans P. Organic Solar Cells with Solution-Processed Graphene Transparent Electrodes. Appl Phys Lett. 2008; 92:263302.
30. Eda G, Fanchini G, Chhowalla M. Large-Area Ultrathin Films of Reduced Graphene Oxide as a Transparent and Flexible Electronic Material. Nat Nanotechnol. 2008; 3:270–274. [PubMed: 18654522]
31. Li XL, Zhang G, Bai X, Sun X, Wang X, Wang E, Dai H. Highly Conducting Graphene Sheets and Langmuir–Blodgett Films. Nat Nanotechnol. 2008; 3:538–542. [PubMed: 18772914]
32. Li JL, Kudin KN, McAllister MJ, Prud'homme RK, Aksay IA, Car R. Oxygen-Driven Unzipping of Graphitic Materials. Phys Rev Lett. 2006; 96:176101. [PubMed: 16712313]
33. Ramanathan T, Abdala AA, Stankovich S, Dikin DA, Herrera-Alonso M, Piner RD, Adamson DH, Schniepp HC, Chen X, Ruoff RS. Functionalized Graphene Sheets for Polymer Nanocomposites. Nat Nanotechnol. 2008; 3:327–331. [PubMed: 18654541]

34. Stankovich S, Piner RD, Nguyen ST, Ruoff RS. Synthesis and Exfoliation of Isocyanate-Treated Graphene Oxide Nanoplatelets. Carbon. 2006; 44:3342–3347.
35. Liu Q, Liu Z, Zhang X, Yang L, Zhang N, Pan G, Yin S, Chen Y, Wei J. Polymer Photovoltaic Cells Based on Solution-Processable Graphene and P3HT. Adv Funct Mater. 2009; 19:894–904.
36. Park S, An J, Jung I, Piner RD, An SJ, Li X, Velamakanni A, Ruoff RS. Colloidal Suspensions of Highly Reduced Graphene Oxide in a Wide Variety of Organic Solvents. Nano Lett. 2009; 9:1593–1597. [PubMed: 19265429]
37. Liang Y, Wu D, Feng X, Mullen K. Dispersion of Graphene Sheets in Organic Solvent Supported by Ionic Interactions. Adv Mater. 2009; 21:1679–1683.
38. Schmidt, W. Hydrazine and Its Derivatives: Preparation, Properties, Applications. Vol. 1. Wiley-Interscience; New York: 2001. Chapter 4
39. Cai MF, Smart RB. Quantitative Analysis of *N*-Methyl-2-pyrrolidinone in Coal Extracts by TGA-FTIR. Energy Fuels. 1993; 7:52–56.
40. White CM, Rohar PC, Veloski GA, Anderson RR. Practical Notes on the Use of *N*-Methyl-2-pyrrolidinone as a Solvent for Extraction of Coal and Coal-Related Materials. Energy Fuels. 1997; 11:1105–1106.
41. Industry calculation reported by Nanocomp INC. Taken from an interview with Nanocomp Inc. CEO, Peter Antoinette: http://nextbigfuture.com/2009/04/interview-with-peter-antoinette.html
42. Ponzio EA, Echevarria R, Morales GM, Barbero C. Removal of *N*-Methylpyrrolidone Hydrogen-Bonded to Polyaniline Free-Standing Films by Protonation–Deprotonation Cycles or Thermal Heating. Polym Int. 2001; 50:1180–1185.
43. Hernandez Y, Nicolosi V, Lotya M, Blighe FM, Sun Z, De S, McGovern IT, Holland B, Byrne M, Gun'Ko YK. High-Yield Production of Graphene by Liquid-Phase Exfoliation of Graphite. Nat Nanotechnol. 2008; 3:563–568. [PubMed: 18772919]
44. Novoselov KS, Geim AK, Morozov SV, Jiang D, Zhang Y, Dubonos SV, Grigorieva IV, Firsov AA. Electric Field Effect in Atomically Thin Carbon Films. Science. 2004; 306:666–669. [PubMed: 15499015]
45. Dikin DA, Stankovich S, Zimney EJ, Piner R, Dommett GHB, Evmenenko G, Nguyen ST, Ruoff RS. Preparation and Characterization of Graphene Oxide Paper. Nature. 2007; 448:457–460. [PubMed: 17653188]
46. Park S, Lee KS, Bozoklu G, Cai W, Nguyen ST, Ruoff RS. Graphene Oxide Papers Modified by Divalent Ions—Enhancing Mechanical Properties *via* Chemical Cross-Linking. ACS Nano. 2008; 2:572–578. [PubMed: 19206584]
47. Buchsteiner A, Lerf A, Pieper J. Water Dynamics in Graphite Oxide Investigated with Neutron Scattering. J Phys Chem B. 2006; 110:22328. [PubMed: 17091972]
48. Lerf A, Buchsteiner A, Pieper J, Schottl S, Dekany I, Szabo T, Boehm HP. Hydration Behavior and Dynamics of Water Molecules in Graphite Oxide. J Phys Chem Solids. 2006; 67:1106–1110.
49. Yang D, Velamakanni A, Bozoklu G, Park S, Piner RD, Stankovich S, Jung I, Field DA, Ventrice JCA, Ruoff RS. Chemical Analysis of Graphene Oxide Films after Heat and Chemical Treatments by X-ray Photoelectron and Micro-Raman Spectroscopy. Carbon. 2009; 47:145–152.
50. At least a portion of the technology which is discussed in this paper is the subject of one or more pending patents.

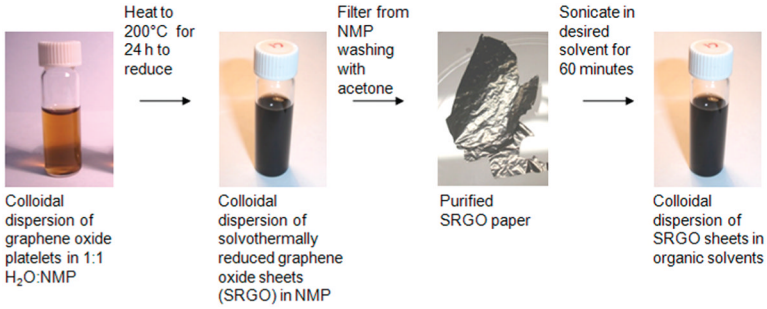

Figure 1.

Schematic diagram shows the preparation and purification of solvothermally reduced graphene oxide (SRGO) to create homogeneous colloidal dispersions of SRGO sheets.

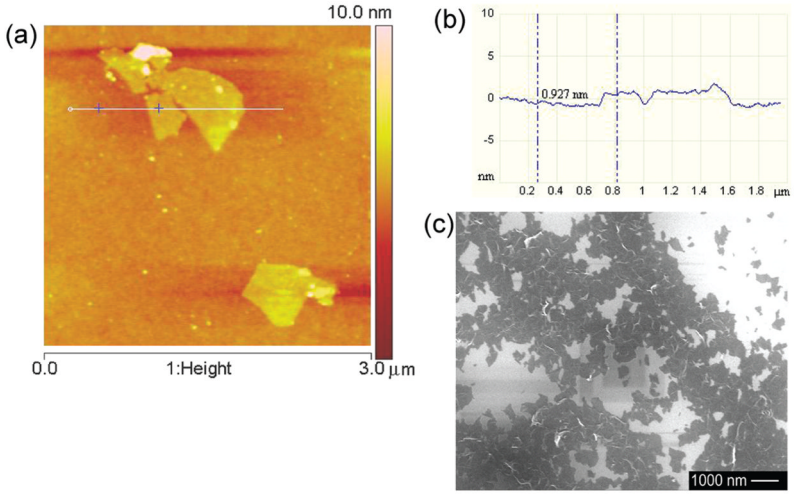

Figure 2.

(a) AFM iimage of SRGO sheets; (b) corresponding AFM height profile from (a) indicates a 0.93 nm sheet thickness. (c) SEM images of SRGO sheets indicate well-dispersed sheets after deposition on Si substrate; inset shows a highly magnified single sheet of SRGO.

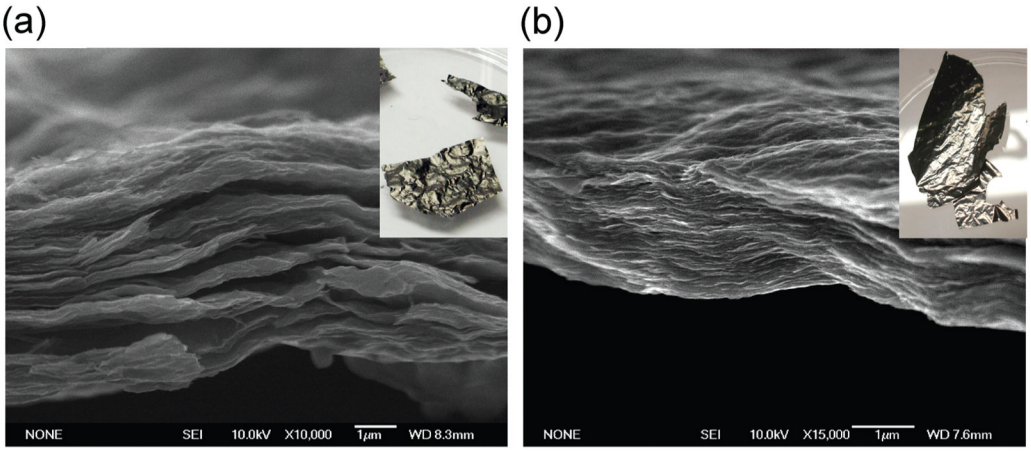

Figure 3.
(a) Scanning electron microscope (SEM) image of a cross-sectional area of the air-dried SRGO film. Inset shows SRGO paper filtered on Anodisc alumina membrane, producing a shiny, black film with metallic-like luster. (b) SEM image of SRGO paper sample annealed at 1000 °C for 12 h under argon indicates that the SRGO paper retains layered structure after annealing. Inset shows SRGO annealed paper gaining a silver/gray appearance after annealing.

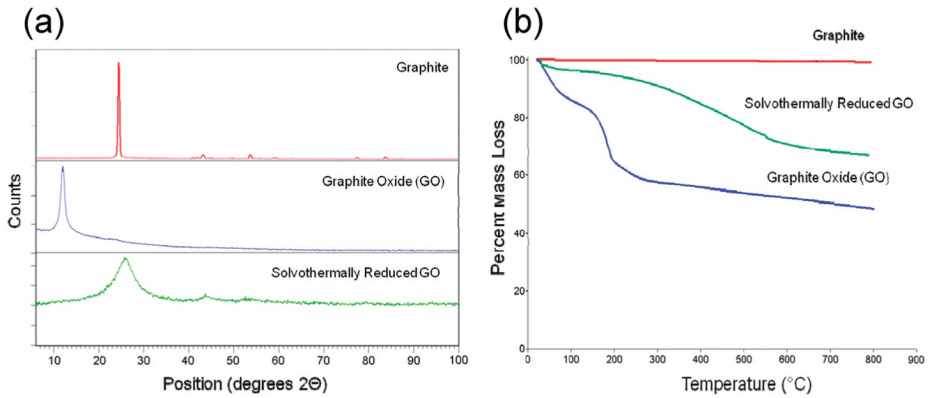

Figure 4.

(a) XRD of graphite (top), graphite oxide (middle), reduced graphite oxide (bottom). (b) Thermal gravimetric analysis (TGA) plot shows a normalized remaining mass of graphite oxide, graphite, and reduced graphite oxide heated under argon.

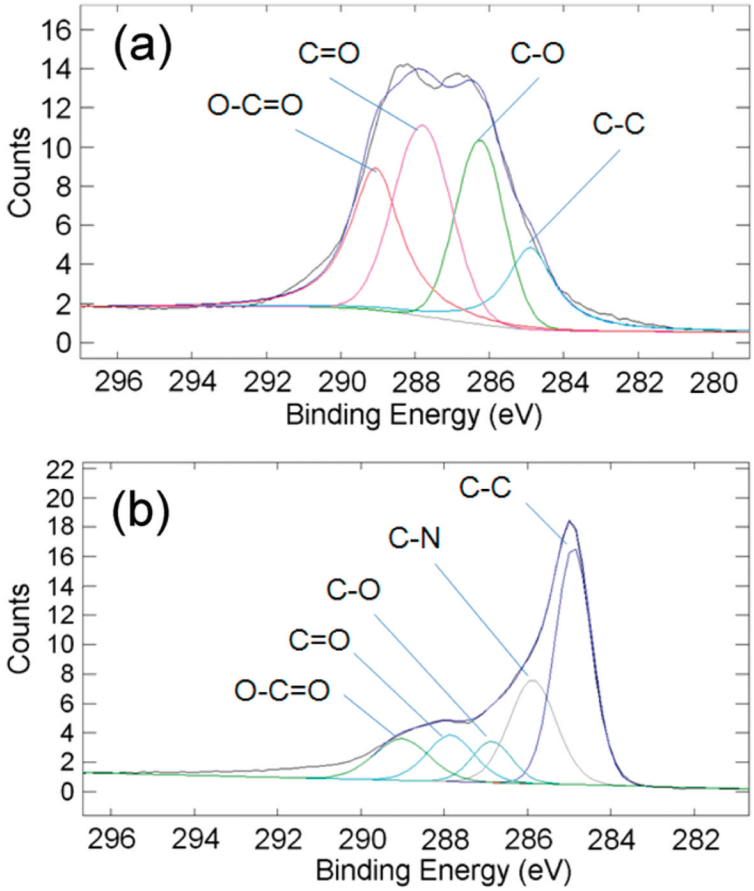

Figure 5.
(a) XPS C1s of GO paper and the corresponding deconvoluted peaks of GO are shown. (b) XPS C1s of air-dried SRGO and the corresponding deconvoluted peaks.

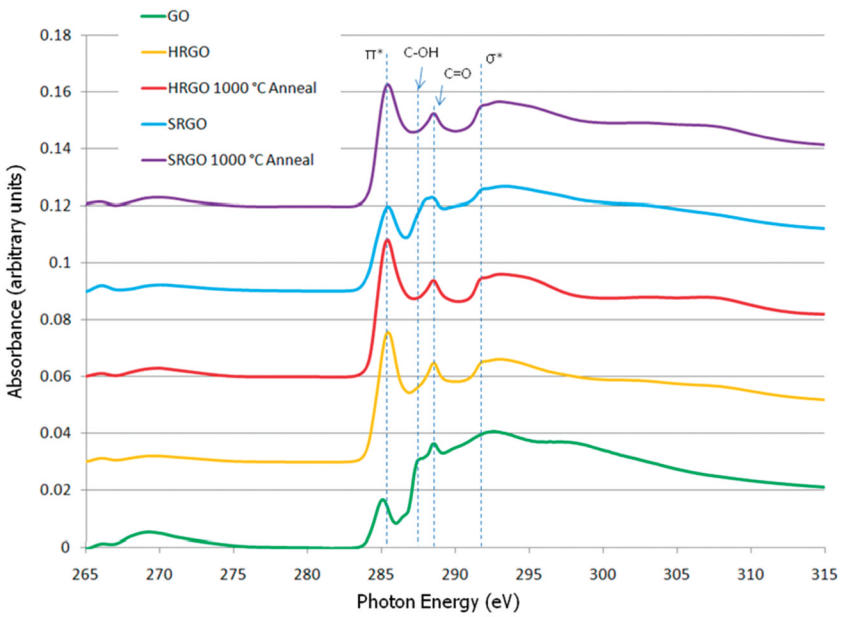

Figure 6.

Overlay plot of the normalized near-edge X-ray absorbance fine structure (NEXAFS) spectra taken at the carbon K-edge for RGOs obtained through various treatments. Each spectrum was taken at 20° incident grazing angle with respect to the X-ray beam. The peak at ~284.5 eV corresponds to the sp^3 carbon π* transition. Smaller peaks at 287.4 and 288.2 eV correspond to oxygen defects. From the overlay, SRGO contains slightly more C–OH with a smaller sp^2 content than HRGO. Annealing SRGO and HRGO at 1000 °C increases the intensity of the π* transition, indicating higher sp^2 content. After annealing, some –C=O content does remain.

TABLE 1

Electrical Conductivities of Solvothermally Reduced Graphite Oxide (RGO) Paper Samples Prepared by Various Methods and Their Comparison to Hydrazine RGO Samples

description	drying conditions	conductivity (S/m)
solvothermal RGO	air-dried	3.74×10^2
	annealed at 250 °C	1.38×10^3
	annealed at 500 °C	5.33×10^3
	annealed at 1000 °C	5.73×10^4
hydrazine RGO[a]	air-dried	8.28×10^3
	annealed at 1000 °C	6.67×10^4
GO boiled in H_2O for 24 h	air-dried	1.00×10^1
GO	air-dried	insulator

[a] Reproduced from Li *et al.*[10]

TABLE 2

List of the Atomic Composition of Solvothermal Reduced Graphite Oxide (RGO) and Hydrazine RGO As Measured by X-ray Photoelectron Spectroscopy (XPS)

description	drying conditions	C (atomic %)	O (atomic %)	N (atomic %)	C/O ratio
solvothermal RGO	air-dried	80.4	15.6	4.0	5.15
solvothermal RGO	annealed at 1000 °C	83.2	13.8	3.0	6.03
hydrazine RGO[a]	air-dried	76.0	21.0	3.0	3.62
hydrazine RGO[a]	annealed at 1000 °C	84.5	13.3	2.2	6.36
GO boiled in H_2O for 24 h	air-dried	75.4	21.1	0.5	3.12
GO	air-dried	69.3	29.3	1.1	2.34

[a]Reproduced from Li *et al.*[10]